Dynamical Viability of Anisotropic Kaniadakis Holographic Dark Energy Models within Brans–Dicke–Rastall Gravity

Y. Aditya et al.

Appendix

Some of the figures are presented here for reference.

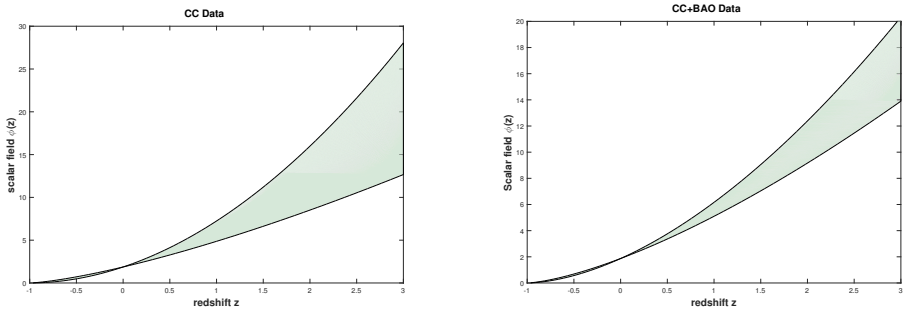

Fig. 3. The plot of the scalar field $\phi(z)$ and redshift z.

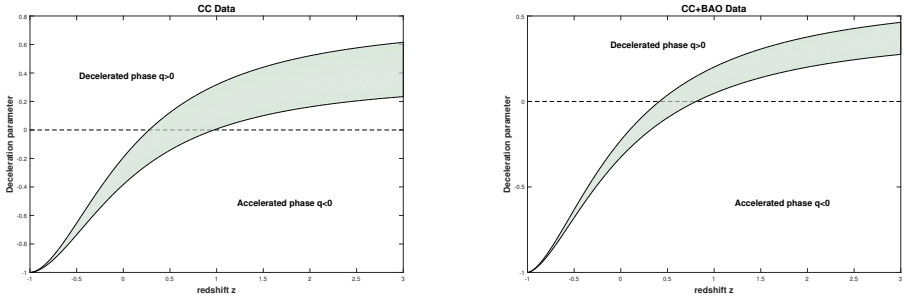

Fig. 4. The plot of the deceleration parameter q versus redshift z.

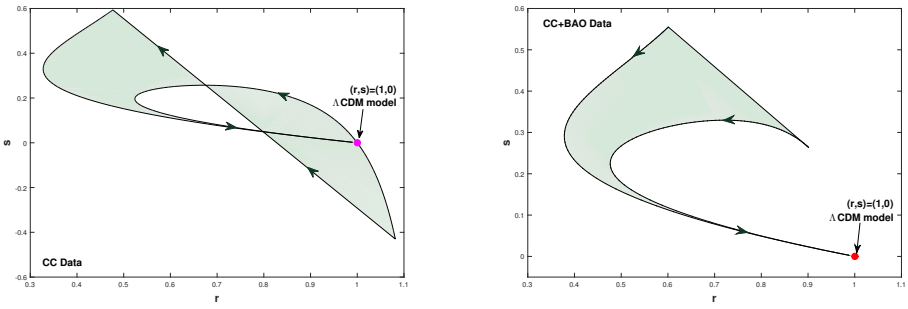

Fig. 5. The plot of statefinder parameters plane.

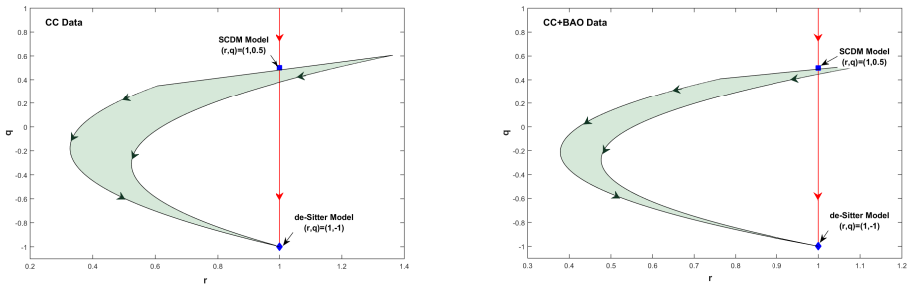

Fig. 6. The plot of the r-q plane.

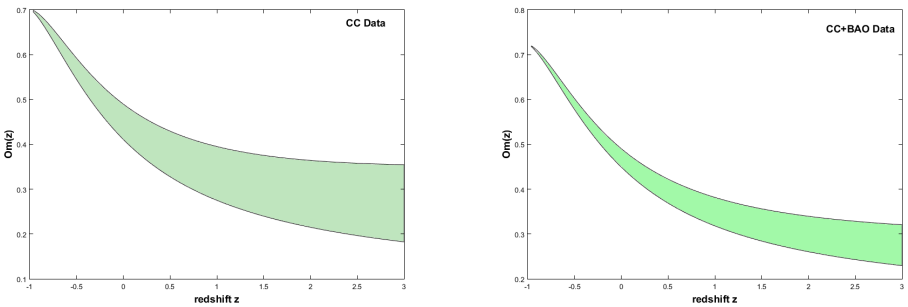

Fig. 7. Evolution of the $Om(z)$ diagnostic with redshift z.

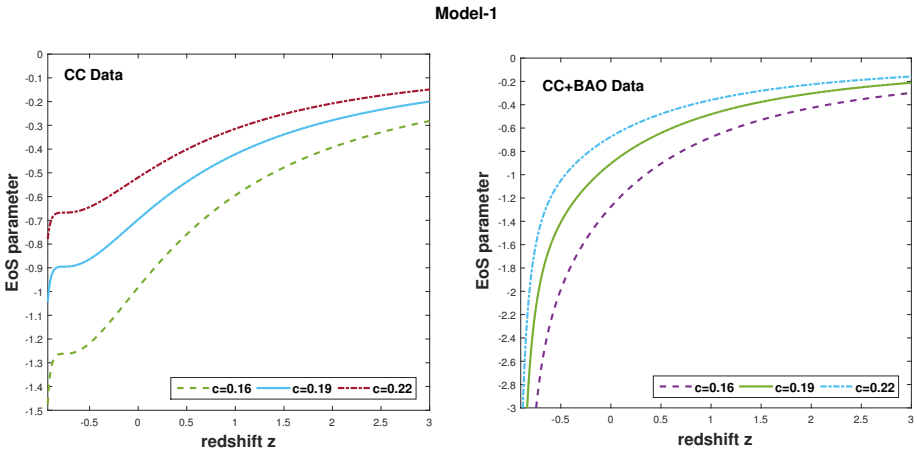

Fig. 8. Plot of the EoS parameter of model-1 versus redshift z.

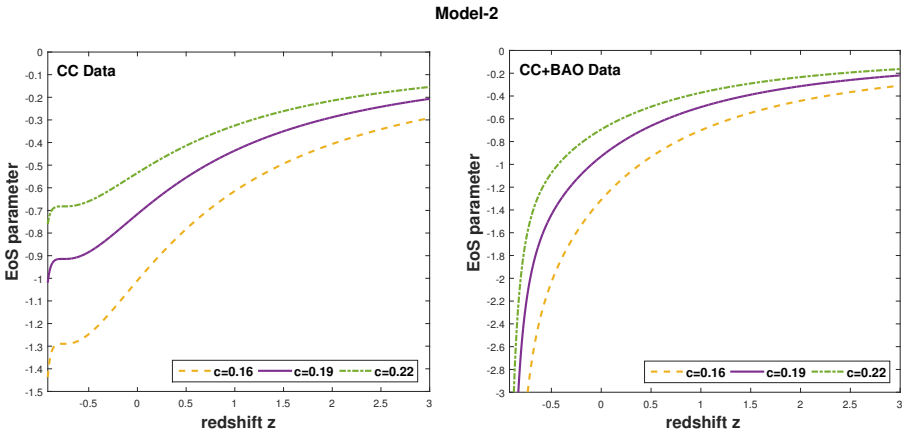

Fig. 9. Plot of the EoS parameter of model-2 versus redshift z.

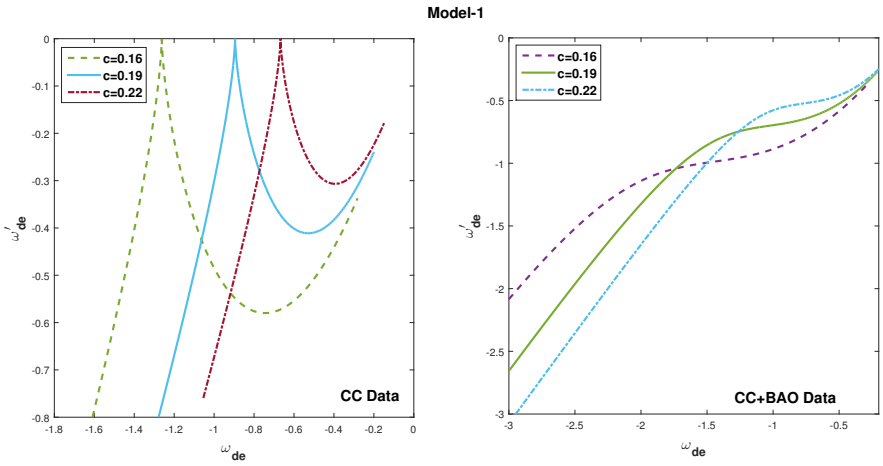

Fig. 10. The plot of the EoS parameter ω_{de} versus its derivative ω'_{de} for model-1.

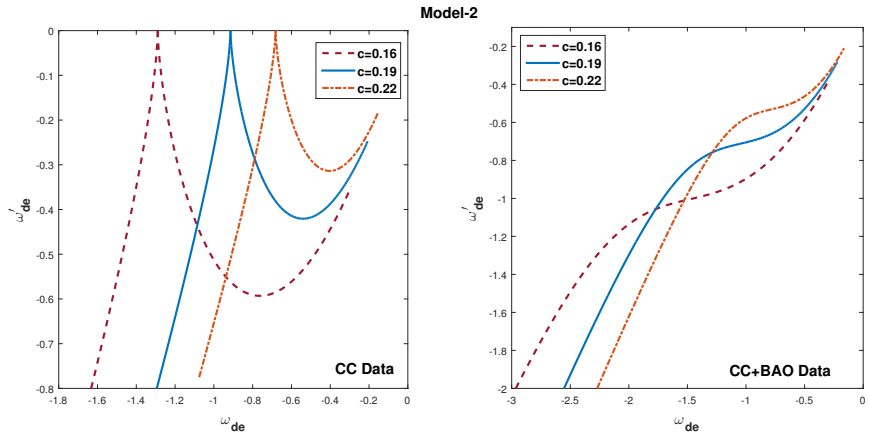

Fig. 11. The plot of the EoS parameter ω_{de} versus its derivative ω'_{de} for model-2.

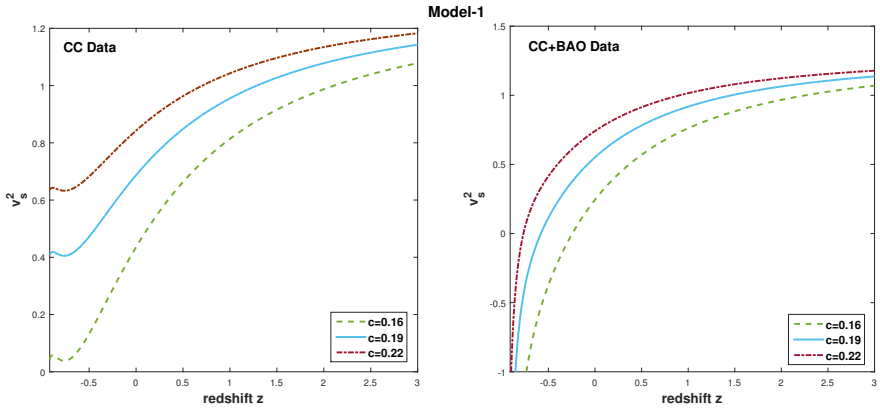

Fig. 12. The plot of the square of the sound speed v_s^2 versus redshift z for model-1.

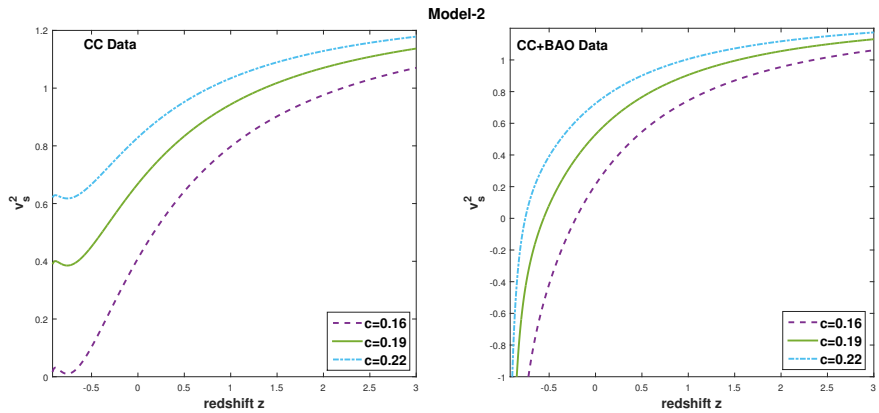

Fig. 13. The plot of the square of the sound speed v_s^2 versus redshift z for model-2.

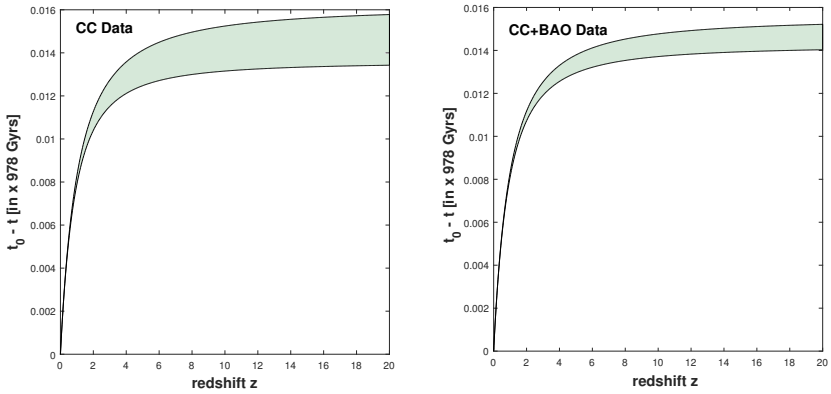

Fig. 14. The plot of the cosmic time difference $t_0 - t$ versus redshift z.

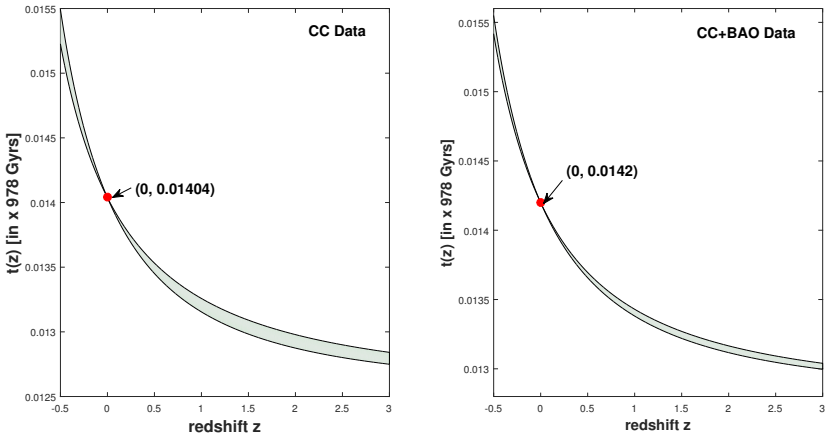

Fig. 15. The plot of the cosmic time $t(z)$ versus redshift z.

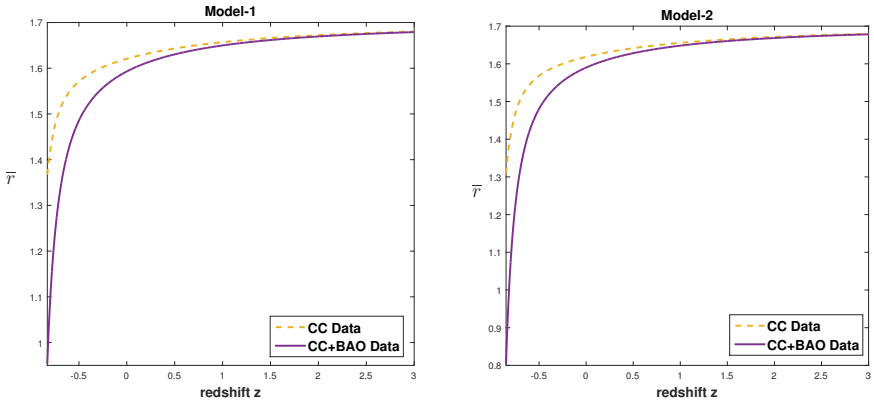

Fig. 16. The plot of the coincidence parameter $\overline{r}$ versus redshift z.

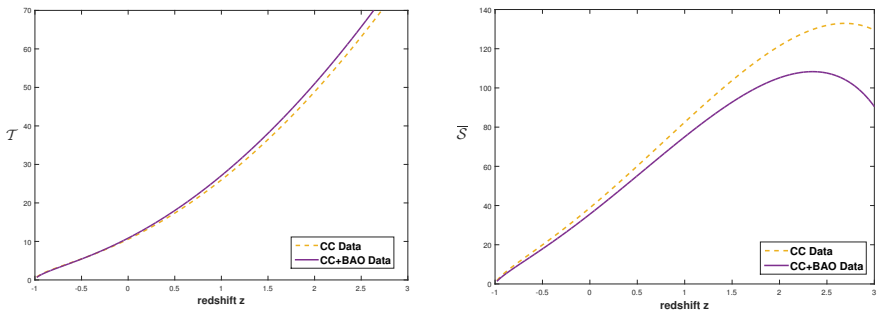

Fig. 17. Plot of entropy density $\mathcal{S}$ and temperature $\mathcal{T}$ versus redshift z for model-1 & 2.